Available online at www.sciencedirect.com
SCIENCE DIRECT®
International Journal of Heat and Mass Transfer 47 (2004) 2173–2182
International Journal of HEAT and MASS TRANSFER
www.elsevier.com/locate/ijhmt

Stability boundary analysis of boiling flow in a narrow vertical annulus heated by counterflow fluids from inner and outer surfaces

Yaojiang Hu [a,*], Huiping Cheng [b]

[a] Institute of Thermophysics Engineering, School of Mechanical and Power Engineering, Shanghai Jiaotong University, Shanghai 200030, PR China

[b] Nuclear Power Engineering Section, Division of Nuclear Power, Department of Nuclear Energy, International Atomic Energy Agency, Vienna, Austria

Received 5 June 2003; received in revised form 22 November 2003

Abstract

The analysis of density wave instability boundary is carried out to investigate the boiling flow in a narrow vertical annular channel, which is heated simultaneously from the inner and the outer sides of the channel by two streams of primary countercurrent flow. The model developed on the basis of the method of weighted residuals, which reduces the channel partial differential equations to seven time-dependent nonlinear ordinary equations, considers the heat-flux coupling between the primary and the secondary channel in space. The derived dynamical system is studied using bifurcation theory to obtain the Hopf bifurcation points, i.e. the stability boundary. The effects of varying the inlet and exit pressure loss coefficients, the inlet subcooling and the system pressure for the channel on the stability boundary are obtained and discussed.

1. Introduction

Two-phase flow instabilities in heated channels have been observed to occur in many industrial systems like conventional and nuclear power plants, refrigeration equipment, and heat exchangers. The thermal oscillations brought about by these instabilities can cause problems of system control and led to the failure of the tube, and therefore are very detrimental to the safe operation of these equipment. It is important to be able to predict the conditions under which a two-phase flow system will be subject to these instabilities in order to leave an adequate margin of safety against oscillations for the equipment. Considered to be the most frequently observed occurrence in boiling channels and of great concern among the various kinds of the two-phase flow instabilities is the density wave instability, which is characterized by the waves of heavier and lighter fluid alternately traveling from the inlet to the outlet channel section. The self-sustained flow oscillation is caused by the coupling between the time delay due to void propagation through the boiling channel and the external feedback pressure drop across the channel.

So far the density wave instability has been extensively studied [1], and considerable interest has already been shifted on from previous analytical work of linear frequency-domain stability analysis of the threshold of instability to recent study of the nonlinear behavior of density wave instability [2–6], which can clarify what happens once the linear-stability threshold has been crossed. Rizwan-Uddin compared the results obtained from different models describing two-phase flow dynamics, i.e., the homogeneous equilibrium model (HEM), the drift-flux model and the two-fluids model, with experimental data for stability boundaries (SB) and

* Corresponding author.
E-mail addresses: ly017107@online.sh.cn (Y. Hu), h.cheng@iaea.org (H. Cheng).

0017-9310/$ - see front matter © 2003 Elsevier Ltd. All rights reserved.
doi:10.1016/j.ijheatmasstransfer.2003.11.011

Nomenclature

A	cross-sectional flow area
D	diameter
Fr	Froude number
f	friction factor
g	gravitational constant
h	enthalpy
k	pressure loss coefficient
L	channel length
N_f	friction number
N_{pch}	phase change number
N_r	$\rho_{\text{f}}^*/(\rho_{\text{f}}^* - \rho_{\text{g}}^*)$
N_{sub}	inlet subcooling number
N_ρ	density ratio
P	pressure
Q	heat transfer rate
q	heat flux
r	radius
T	temperature
t	time
U	overall heat transfer coefficient
v	velocity
x	quality
z	coordinate along the channel

Greek symbols

α	void fraction
β	frequency
η	boiling dryout boundary
μ	boiling inception boundary
ρ	density
ξ	perimeter

Subscripts

1	superheated vapor region
2	two-phase region
3	subcooled liquid region
acc	acceleration
b	secondary side (the channel)
exit	channel exit
ext	external
f	primary side or liquid
fric	frictional
g	vapor
grav	gravitational
inlet	channel inlet
m	mixture

verified that the simple HEM could also yield very good agreement [5]. Karve studied the nuclear-coupled thermal-hydraulic stability of boiling water reactors using the method of weighted residuals (MWR) to reduce the channel PDEs of HEM to a set of nonlinear ODEs and validated that quadratic profiles for single-phase enthalpy and two-phase quality are sufficient and are the best compromise between the simplicity of the model and the accuracy of the results for SB [7]. The inherent local linear-stability information for the ODEs can be readily obtained by calculating its eigenvalues whereas the model can still be applied to reveal the nonlinear effects.

In view of the importance of the linear-stability analysis of the threshold of instability and the extensibility to further include nonlinear effects, Karve's model is therefore adopted and developed in this paper to describe the forced-flow boiling in a concentric circular-tube narrow annulus heated by primary high temperature fluids from the inner surface and the outer surface simultaneously. The steady-state solutions, i.e., the heat fluxes for the three regions of the channel which are required by our SB analyses, are provided by our previous calculation results [8]. The derived dynamical system is studied using bifurcation theory to obtain the Hopf bifurcation points, which compose the stability boundary. The effects of varying the inlet and exit pressure loss coefficients, the inlet subcooling and the system pressure for the channel on the stability boundary are obtained and discussed. The work reported here is also a further step toward our eventual goal, i.e., the development of a nonlinear dynamic model which is capable of dealing with the dynamic coupling between the primary and secondary fluids of the once-though steam generator in this configuration.

2. Analysis

2.1. The model

The concentric circular-tube annulus is schematically shown in Fig. 1. Driven by the external pressure difference, the secondary subcooled water enters into the annular channel from bottom and flows upwards, meanwhile, it is heated along the channel through inner wall and outer wall by the two streams of counterflow primary liquid water at high temperature, which flow respectively through the inner tube and the annular duct (insulated on the exterior wall) outside the outer tube. The secondary water will begin to boil at position μ, dry out at position η, and reaches the exit as superheated vapor. Accordingly the annular channel can be divided into three regions, i.e., subcooled single-phase region,

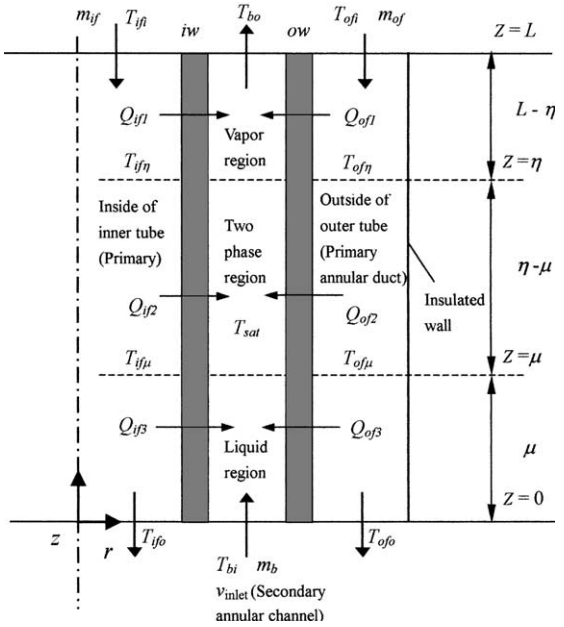

Fig. 1. Configuration of annular channel.

two-phase region and superheated single-phase region. Other notation in Fig. 1 can be readily understood and referred to in the Nomenclature. In addition, the one-dimensional HEM for two-phase flow is assumed for the physical system.

The main extensions to Karve's model in this paper are the addition of the superheated vapor region which results in the two additional equations for the distribution of the enthalpy for the region, and the revision of the heating condition for the channel to incorporate our previous steady-state results into the SB analysis.

The procedures to derive the dynamic system for the forced flow in the annulus are that first the one-dimensional time-dependent energy conservation equations in the two single-phase regions and the HEM equations in the two-phase region are given, then the quadratic spatial approximations for these single-phase enthalpies and the two-phase quality are made, and the MWR is used to reduce the channel PDEs to ODEs, finally an ODE describing the relation between the channel inlet velocity and the external pressure drop is derived from the channel momentum conservation equations. In total the dynamic system consists of seven ODEs. These are for the phase variables $a_1(t)$, $a_2(t)$, $s_1(t)$, $s_2(t)$, $b_1(t)$, $b_2(t)$ and $v_{\text{inlet}}(t)$ in the channel. The variables $a_1(t)$ and $a_2(t)$ are respectively the coefficients of the linear and quadratic terms of the spatially quadratic representation for the space- and time-dependent single-phase subcooled enthalpy. The variables $s_1(t)$ and $s_2(t)$ are respectively the coefficients of the linear and quadratic terms of the spatially quadratic representation for the space- and time-dependent two-phase quality. The variables $b_1(t)$ and $b_2(t)$ are respectively the coefficients of the linear and quadratic terms of the spatially quadratic representation for the space- and time-dependent single-phase superheated enthalpy. The variable $v_{\text{inlet}}(t)$ is the channel inlet velocity. The seven ODEs are derived below.

2.1.1. ODEs for $a_1(t)$ and $a_2(t)$ in the subcooled liquid region

The enthalpy equation for the incompressible subcooled liquid phase is

$$\rho_{\text{f}}^{*}\frac{\partial h^{*}(z^{*},t^{*})}{\partial t^{*}}+\rho_{\text{f}}^{*}v_{\text{inlet}}^{*}(t^{*})\frac{\partial h^{*}(z^{*},t^{*})}{\partial z^{*}}=\frac{q_{\text{if3}}^{*}\xi_{\text{iwo}}^{*}+q_{\text{of3}}^{*}\xi_{\text{owi}}^{*}}{A_{\text{b}}^{*}}, \tag{1}$$

where A_{b}^{*} is the cross-sectional area for the channel, i.e.,

$$A_{\text{b}}^{*}=\pi(r_{\text{owi}}^{*^2}-r_{\text{iwo}}^{*^2}). \tag{2}$$

ξ_{iwo}^{*} and ξ_{owi}^{*} are respectively the wetted perimeters for the inner and outer walls of the channel, i.e.,

$$\xi_{\text{iwo}}^{*}=2\pi r_{\text{iwo}}^{*}, \tag{3}$$

$$\xi_{\text{owi}}^{*}=2\pi r_{\text{owi}}^{*}. \tag{4}$$

h^{*} is the subcooled single-phase enthalpy, q_{if3}^{*} and q_{of3}^{*} are the heat fluxes of the inner and outer walls in the region, which are respectively calculated from our previous steady-state analysis as

$$q_{\text{if3}}^{*}=U_{\text{iwo3}}^{*}\frac{(T_{\text{ifo}}^{*}-T_{\text{bi}}^{*})-(T_{\text{if}\mu}^{*}-T_{\text{sat}}^{*})}{\ln\frac{T_{\text{ifo}}^{*}-T_{\text{bi}}^{*}}{T_{\text{if}\mu}^{*}-T_{\text{sat}}^{*}}}, \tag{5}$$

$$q_{\text{of3}}^{*}=U_{\text{owi3}}^{*}\frac{(T_{\text{ofo}}^{*}-T_{\text{bi}}^{*})-(T_{\text{of}\mu}^{*}-T_{\text{sat}}^{*})}{\ln\frac{T_{\text{ofo}}^{*}-T_{\text{bi}}^{*}}{T_{\text{of}\mu}^{*}-T_{\text{sat}}^{*}}}. \tag{6}$$

By introducing the following dimensionless variables

$$\begin{aligned}
&h(z,t)=\frac{h^{*}(z^{*},t^{*})}{\Delta h_{\text{fg}}^{*}},\quad t=\frac{t^{*}v_{0}^{*}}{L^{*}},\quad z=\frac{z^{*}}{L^{*}},\\
&v_{\text{inlet}}(t)=\frac{v_{\text{inlet}}^{*}}{v_{0}^{*}},\quad T=\frac{T^{*}}{T_{0}^{*}}\quad N_{\rho}=\frac{\rho_{\text{g}}^{*}}{\rho_{\text{f}}^{*}},\\
&N_{r}=\frac{\rho_{\text{f}}^{*}}{\Delta\rho^{*}},\quad N_{\text{pch3}}=\frac{L^{*}\Delta\rho^{*}(q_{\text{if3}}^{*}\xi_{\text{iwo}}^{*}+q_{\text{of3}}^{*}\xi_{\text{owi}}^{*})}{A_{\text{b}}^{*}\Delta h_{\text{fg}}^{*}\rho_{\text{f}}^{*}\rho_{\text{g}}^{*}v_{0}^{*}},
\end{aligned} \tag{7}$$

Eq. (1) can be rearranged into the following dimensionless form

$$\frac{\partial h(z,t)}{\partial t}+v_{\text{inlet}}(t)\frac{\partial h(z,t)}{\partial z}=N_{\rho}N_{r}N_{\text{pch3}}, \tag{8}$$

where T_{0}^{*} and v_{0}^{*} are respectively the reference temperature and the reference velocity, and N_{pch3} is the phase change number for the region.

As the same method taken in Karve's model we approximate $h(z,t)$ by the following quadratic function $h_{N}(z,t)$ as

$$h(z,t) \approx h_N(z,t) = h_{\text{inlet}} + a_1(t)z + a_2(t)z^2 \tag{9}$$

and take the weight functions as unity and z respectively, then use MWR to obtain the following two ODEs as

$$\frac{\mathrm{d}a_1(t)}{\mathrm{d}t} = \frac{6}{\mu(t)}\left[N_\rho N_r N_{\text{pch3}} - v_{\text{inlet}}(t)a_1(t)\right] - 2v_{\text{inlet}}(t)a_2(t), \tag{10}$$

$$\frac{\mathrm{d}a_2(t)}{\mathrm{d}t} = -\frac{6}{\mu^2(t)}\left[N_\rho N_r N_{\text{pch3}} - v_{\text{inlet}}(t)a_1(t)\right]. \tag{11}$$

At steady state we have

$$\tilde{a}_1 = \frac{N_\rho N_r N_{\text{pch3}}}{\tilde{v}_{\text{inlet}}}, \tag{12}$$

$$\tilde{a}_2 = 0 \tag{13}$$

and the enthalpy profile becomes linear.

By substituting the boundary condition

$$h(\mu(t),t) = h_{\text{sat}} \tag{14}$$

into Eq. (9), the boiling inception boundary $\mu(t)$ could be obtained as

$$\mu(t) = \frac{2N_\rho N_r N_{\text{sub}}}{a_1(t) + \sqrt{a_1^2(t) + 4a_2(t)N_\rho N_r N_{\text{sub}}}}, \tag{15}$$

where the inlet subcooled number is defined as

$$N_{\text{sub}} = \frac{(h^*_{\text{sat}} - h^*_{\text{inlet}})\Delta\rho^*}{\Delta h^*_{\text{fg}}\rho^*_{\text{g}}}. \tag{16}$$

The physical meaning for Eq. (15) can be clearly seen by substituting Eqs. (12) and (13) into it and converting the resulting equation into its dimensional form as

$$\tilde{q}^*_{\text{if3}}\xi^*_{\text{iwo}}\tilde{\mu} + \tilde{q}^*_{\text{of3}}\xi^*_{\text{owi}}\tilde{\mu} = \rho^*_{\text{f}}\tilde{v}^*_{\text{inlet}}A^*_{\text{b}}(h^*_{\text{sat}} - h^*_{\text{inlet}}), \tag{17}$$

i.e.,

$$Q^*_{\text{if3}} + Q^*_{\text{of3}} = m^*_{\text{b}}(h^*_{\text{sat}} - h^*_{\text{inlet}}), \tag{18}$$

which is exactly the same energy conservation equation as that in our previous steady-state flow analysis [8].

2.1.2. ODEs for $s_1(t)$ and $s_2(t)$ in the two-phase region

For the HEM, the two-phase mixture density equation is

$$\frac{\partial\rho^*_{\text{m}}(z^*,t^*)}{\partial t^*} + \frac{\partial}{\partial z^*}\left[\rho^*_{\text{m}}(z^*,t^*)v^*_{\text{m}}(z^*,t^*)\right] = 0, \tag{19}$$

where the relation between $\rho^*_{\text{m}}(z^*,t^*)$ and the void fraction $\alpha(z^*,t^*)$ is

$$\rho^*_{\text{m}}(z^*,t^*) = \alpha(z^*,t^*)\rho^*_{\text{g}} + [1-\alpha(z^*,t^*)]\rho^*_{\text{f}} \tag{20}$$

and $\alpha(z^*,t^*)$ is related to the mixture quality $x(z^*,t^*)$ as

$$\alpha(z^*,t^*) = \frac{1}{1 + \frac{1-x}{x}\frac{\rho^*_{\text{g}}}{\rho^*_{\text{f}}}}. \tag{21}$$

In Eq. (19) the mixture velocity $v^*_{\text{m}}(z^*,t^*)$ satisfies

$$\frac{\partial v^*_{\text{m}}(z^*,t^*)}{\partial z^*} = \frac{(q^*_{\text{if2}}\xi^*_{\text{iwo}} + q^*_{\text{of2}}\xi^*_{\text{owi}})\Delta\rho^*}{\rho^*_{\text{f}}\rho^*_{\text{g}}A^*_{\text{b}}\Delta h^*_{\text{fg}}}, \tag{22}$$

where q^*_{if2} and q^*_{of2} are respectively the heat fluxes of the inner and outer walls in the two-phase region and provided by our previous analysis as

$$q^*_{\text{if2}} = U^*_{\text{iwo2}}\frac{T^*_{\text{if}\eta} - T^*_{\text{if}\mu}}{\ln\dfrac{T^*_{\text{if}\eta} - T^*_{\text{sat}}}{T^*_{\text{if}\mu} - T^*_{\text{sat}}}}, \tag{23}$$

$$q^*_{\text{of2}} = U^*_{\text{owi2}}\frac{T^*_{\text{of}\eta} - T^*_{\text{of}\mu}}{\ln\dfrac{T^*_{\text{of}\eta} - T^*_{\text{sat}}}{T^*_{\text{of}\mu} - T^*_{\text{sat}}}}. \tag{24}$$

Introducing the two additional dimensionless variables

$$\rho_{\text{m}}(z,t) = \frac{\rho^*_{\text{m}}(z^*,t^*)}{\rho^*_{\text{f}}}, \quad v_{\text{m}}(z,t)\frac{v^*_{\text{m}}}{v^*_0} \tag{25}$$

and through Eq. (22), we can transform Eq. (19) into the following dimensionless form as

$$\frac{\partial\rho_{\text{m}}(z,t)}{\partial t} + v_{\text{m}}(z,t)\frac{\partial\rho_{\text{m}}(z,t)}{\partial z} = -N_{\text{pch2}}\rho_{\text{m}}(z,t), \tag{26}$$

where the phase change number N_{pch2} for the two-phase region is

$$N_{\text{pch2}} = \frac{(q^*_{\text{if2}}\xi_{\text{iwo}} + q^*_{\text{of2}}\xi^*_{\text{owi}})L^*\Delta\rho^*}{A^*_{\text{b}}\Delta h^*_{\text{fg}}\rho^*_{\text{f}}\rho^*_{\text{g}}v^*_0} \tag{27}$$

and $\rho_{\text{m}}(z,t)$ can be written through Eqs. (20) and (21) as

$$\rho_{\text{m}}(z,t) = \frac{N_\rho N_r}{N_\rho N_r + x(z,t)}. \tag{28}$$

The dimensionless mixture velocity is obtained by integrating Eq. (22) from $\mu(t)$ to any z in the two-phase region as

$$v_{\text{m}}(z,t) = v_{\text{inlet}}(t) + N_{\text{pch2}}[z - \mu(t)]. \tag{29}$$

As the same in Karve's model $x(z,t)$ is approximated by the quadratic function $x_2(z,t)$ as

$$x(z,t) \approx x_2(z,t) = N_\rho N_r\{s_1(t)[z-\mu(t)] + s_2(t)[z-\mu(t)]^2\} \tag{30}$$

and the two weight functions are taken as unity and $z-\mu(t)$ respectively, then the following two ODEs can be obtained by using MWR as

$$\frac{\mathrm{d}s_1(t)}{\mathrm{d}t} = \frac{1}{f_2(t)}\left[f_3(t)f_1(t) + f_4(t)\right], \tag{31}$$

$$\frac{\mathrm{d}s_2(t)}{\mathrm{d}t} = \frac{1}{f_2(t)}\left[f_5(t)f_1(t) + f_6(t)\right]. \tag{32}$$

Here the limits of integration for the inner product in using MWR are from $z = \mu(t)$ to $z = \eta(f)$, which is

different from that in Karve's model, and the boiling dryout boundary $\eta(t)$ is given by

$$\eta(t) = \mu(t) + \frac{2}{N_\rho N_r\left(\sqrt{s_1^2(t) + \frac{4s_2(t)}{N_\rho N_r}} + s_1(t)\right)}, \tag{33}$$

which is obtained by applying the boundary condition $x(\eta(t), t) = 1$ to Eq. (30).

At steady state we have

$$\tilde{s}_1 = \frac{N_{\text{pch2}}}{\tilde{v}_{\text{inlet}}}, \tag{34}$$

$$\tilde{s}_2 = 0. \tag{35}$$

In the similar way we can check that, when at steady state, Eq. (33) is degraded as exactly the same as the steady-state energy conservation equation describing the two-phase flow in the region, which is used in our previous steady-state analysis.

The intermediate functions in Eqs. (31) and (32) are the same as that in Karve's analysis [7] except for the limits of integration. They are

$$\begin{aligned}
f_1(t) &= \frac{\mathrm{d}\mu(t)}{\mathrm{d}t},\\
f_2(t) &= I_3^2(t) - I_1(t)I_6(t),\\
f_3(t) &= s_1(t)[I_1(t)I_3(t) - I_2(t)I_6(t)]\\
&\quad + 2s_2(t)[I_3^2(t) - I_1(t)I_6(t)],\\
f_4(t) &= N_{\text{pch2}}[M_2(t)I_3(t) - M_1(t)I_6(t)]\\
&\quad - v_{\text{inlet}}(t)s_1(t)[I_1(t)I_3(t) - I_2(t)I_6(t)]\\
&\quad - [2v_{\text{inlet}}(t)s_2(t) + N_{\text{pch2}}(t)s_1(t)]\\
&\quad \times [I_3^2(t) - I_1(t)I_6(t)],\\
f_5(t) &= s_1(t)[I_2(t)I_3(t) - I_1^2],\\
f_6(t) &= N_{\text{pch2}}[M_1(t)I_3(t) - M_2(t)I_1(t)]\\
&\quad - v_{\text{inlet}}(t)s_1(t)[I_2(t)I_3(t) - I_1^2(t)]\\
&\quad - 2s_2N_{\text{pch2}}[I_3^2(t) - I_1(t)I_6(t)].
\end{aligned}$$

$$\begin{aligned}
I_1(t) &= \int_{\mu(t)}^{\eta(t)} \frac{z-\mu(t)}{\{1+s_1(t)[z-\mu(t)]+s_2(t)[z-\mu(t)]^2\}^2}\,\mathrm{d}z,\\
I_2(t) &= \int_{\mu(t)}^{\eta(t)} \frac{1}{\{1+s_1(t)[z-\mu(t)]+s_2(t)[z-\mu(t)]^2\}^2}\,\mathrm{d}z,\\
I_3(t) &= \int_{\mu(t)}^{\eta(t)} \frac{[z-\mu(t)]^2}{\{1+s_1(t)[z-\mu(t)]+s_2(t)[z-\mu(t)]^2\}^2}\,\mathrm{d}z,\\
I_6(t) &= \int_{\mu(t)}^{\eta(t)} \frac{[z-\mu(t)]^3}{\{1+s_1(t)[z-\mu(t)]+s_2(t)[z-\mu(t)]^2\}^2}\,\mathrm{d}z,\\
M_1(t) &= \int_{\mu(t)}^{\eta(t)} \frac{1}{1+s_1(t)[z-\mu(t)]+s_2(t)[z-\mu(t)]^2}\,\mathrm{d}z,\\
M_2(t) &= \int_{\mu(t)}^{\eta(t)} \frac{z-\mu(t)}{1+s_1(t)[z-\mu(t)]+s_2(t)[z-\mu(t)]^2}\,\mathrm{d}z.
\end{aligned} \tag{36}$$

2.1.3. ODEs for $b_1(t)$ and $b_2(t)$ in the superheated vapor region

The dimensionless enthalpy equation for the superheated vapor region is

$$\frac{\partial h(z,t)}{\partial t} + v_{\text{m}}(\eta(t),t)\frac{\partial h(z,t)}{\partial z} = N_r N_{\text{pch1}}, \tag{37}$$

where

$$N_{\text{pch1}} = \frac{(q^*_{\text{if1}}\xi^*_{\text{iwo}} + q^*_{\text{of1}}\xi^*_{\text{owi}})L^*\Delta\rho^*}{A^*_{\text{b}}\Delta h^*_{\text{fg}}\rho^*_{\text{g}}\rho^*_{\text{f}}v^*_0}, \tag{38}$$

$$q^*_{\text{if1}} = U^*_{\text{iwo1}}\frac{(T^*_{\text{if}\eta} - T^*_{\text{sat}}) - (T^*_{\text{ifi}} - T^*_{\text{bo}})}{\ln\dfrac{T^*_{\text{if}\eta} - T^*_{\text{sat}}}{T^*_{\text{ofi}} - T^*_{\text{bo}}}}, \tag{39}$$

$$q^*_{\text{of1}} = U^*_{\text{owi1}}\frac{(T^*_{\text{of}\eta} - T^*_{\text{sat}}) - (T^*_{\text{ofi}} - T^*_{\text{bo}})}{\ln\dfrac{T^*_{\text{of}\eta} - T^*_{\text{sat}}}{T^*_{\text{ofi}} - T^*_{\text{bo}}}}. \tag{40}$$

In a similar way in using MWR we introduce two vector operators

$$\mathbf{A} = \frac{\partial}{\partial t} + v_{\text{m}}(\eta(t),t)\frac{\partial}{\partial z}, \tag{41}$$

$$\mathbf{S} = N_r N_{\text{pch1}} \tag{42}$$

and approximate a quadratic profile for the enthalpy in the region as

$$\begin{aligned}
h(z,t) &\approx h_2(z,t)\\
&= h_{\text{sat}v} + b_1(t)[z-\eta(t)] + b_2(t)[z-\eta(t)]^2
\end{aligned} \tag{43}$$

and substitute the weight functions $w_1(z) = 1$ and $w_2(z) = z - \eta(t)$ respectively into the following equations

$$(w_k, \{\mathbf{A}h_2 - \mathbf{S}\}) = 0, \quad (k = 1, 2) \tag{44}$$

to arrive at the two equations.

In Eq. (44) the inner product is represented as

$$(\alpha, \beta) = \int_{\eta(t)}^{1} \alpha(z)\beta(z)\,\mathrm{d}z. \tag{45}$$

By solving the resulting two linear equations simultaneously for the derivatives for $b_1(t)$ and $b_2(t)$, we obtain

$$\begin{aligned}
\frac{\mathrm{d}b_1(t)}{\mathrm{d}t} &= \frac{6}{1-\eta(t)}\left\{N_r N_{\text{pch1}} - \left[v_{\text{m}}(\eta(t),t) - \frac{\mathrm{d}\eta(t)}{\mathrm{d}t}\right]b_1(t)\right\}\\
&\quad - 2\left[v_{\text{m}}(\eta(t),t) - \frac{\mathrm{d}\eta(t)}{\mathrm{d}t}\right]b_2(t),
\end{aligned} \tag{46}$$

$$\frac{\mathrm{d}b_2(t)}{\mathrm{d}t} = \frac{-6}{[1-\eta(t)]^2}\left\{N_r N_{\text{pch1}} - \left[v_{\text{m}}(\eta(t),t) - \frac{\mathrm{d}\eta(t)}{\mathrm{d}t}\right]b_1(t)\right\}. \tag{47}$$

We can see that Eqs. (46) and (47) are like Eqs. (10) and (11) respectively in their forms.

In Eqs. (46) and (47) the mixture velocity at the dryout position is

$$v_{\mathrm{m}}(\eta(t),t) = v_{\mathrm{inlet}}(t) + N_{\mathrm{pch2}}[\eta(t) - \mu(t)]. \tag{48}$$

At steady state we have

$$\tilde{b}_1 = \frac{N_\rho N_r N_{\mathrm{pch1}}}{\tilde{v}_{\mathrm{inlet}}}, \tag{49}$$

$$\tilde{b}_2 = 0. \tag{50}$$

2.1.4. ODE for $v_{inlet}(t)$ in the channel

The ODE describing the relation between the channel inlet velocity $v_{\mathrm{inlet}}(t)$ and the external pressure drop ΔP_{ext} is derived from the momentum conservation equations for the three regions.

The three momentum equations are respectively written as

$$-\frac{\partial P_3^*}{\partial z^*} = \rho_{\mathrm{f}}^*\left[\frac{\mathrm{d}v_{\mathrm{inlet}}^*(t^*)}{\mathrm{d}t^*} + \frac{f_3^*}{2D_h^*}v_{\mathrm{inlet}}^{*2}(t^*) + g^*\right], \tag{51}$$

$$-\frac{\partial P_2^*}{\partial z^*} = \rho_{\mathrm{m}}^*(z^*,t^*)\left[\frac{\partial v_{\mathrm{m}}^*(z^*,t^*)}{\partial t^*} + v_{\mathrm{m}}^*(z^*,t^*)\frac{\partial v_{\mathrm{m}}^*(z^*,t^*)}{\partial z^*} + \frac{f_2^*}{2D_h^*}v_{\mathrm{m}}^{*2}(z^*,t^*) + g^*\right], \tag{52}$$

$$-\frac{\partial P_1^*}{\partial z^*} = \rho_{\mathrm{g}}^*\left[\frac{\mathrm{d}v_{\mathrm{m}}^*(\eta^*(t^*),t^*)}{\mathrm{d}t^*} + \frac{f_1^*}{2D_h^*}v_{\mathrm{m}}^{*2}(\eta^*(t^*),t^*) + g^*\right], \tag{53}$$

where the equivalent hydraulic diameter is

$$D_h^* = \frac{4A_{\mathrm{b}}^*}{\xi_{\mathrm{iwo}}^* + \xi_{\mathrm{owi}}^*}. \tag{54}$$

The dimensionless forms for Eqs. (51)–(53) are respectively

$$-\frac{\partial P_3}{\partial z} = \frac{\mathrm{d}v_{\mathrm{inlet}}(t)}{\mathrm{d}t} + N_{f3}v_{\mathrm{inlet}}^2 + Fr^{-1}, \tag{55}$$

$$-\frac{\partial P_2}{\partial z} = \rho_{\mathrm{m}}(z,t)\left[\frac{\partial v_{\mathrm{m}}(z,t)}{\partial t} + v_{\mathrm{m}}(z,t)\frac{\partial v_{\mathrm{m}}(z,t)}{\partial z} + N_{f2}v_{\mathrm{m}}^2(z,t) + Fr^{-1}\right], \tag{56}$$

$$-\frac{\partial P_1}{\partial z} = N_\rho\left[\frac{\mathrm{d}v_{\mathrm{m}}(\eta(t),t)}{\mathrm{d}t} + N_{f1}v_{\mathrm{m}}^2(\eta(t),t) + Fr^{-1}\right], \tag{57}$$

where the dimensionless variables in the above equations are

$$P_j = \frac{P_j^*}{\rho_{\mathrm{f}}^* v_0^{*2}}, \quad N_{fj} = \frac{f_j^* L^*}{2D_h^*}, \quad (j = 1,2,3), \quad Fr = \frac{v_0^{*2}}{g^* L^*}. \tag{58}$$

The pressure drop $\Delta P_3(t)$ across the subcooled liquid region can be obtained by integrating Eq. (55) from $z = 0$ to $z = \mu(t)$ as

$$\Delta P_3(t) = \Delta P_{\mathrm{acc},3}(t) + \Delta P_{\mathrm{fric},3}(t) + \Delta P_{\mathrm{grav},3}(t), \tag{59}$$

where

$$\Delta P_{\mathrm{acc},3} = \int_0^{\mu(t)} \frac{\mathrm{d}v_{\mathrm{inlet}}(t)}{\mathrm{d}t}\,\mathrm{d}z = \mu(t)\frac{\mathrm{d}v_{\mathrm{inlet}}(t)}{\mathrm{d}t}, \tag{60}$$

$$\Delta P_{\mathrm{fric},3} = \int_0^{\mu(t)} N_{f3}v_{\mathrm{inlet}}^2(t)\,\mathrm{d}z = N_{f3}v_{\mathrm{inlet}}^2(t)\mu(t), \tag{61}$$

$$\Delta P_{\mathrm{grav},3} = \int_0^{\mu(t)} Fr^{-1}\,\mathrm{d}z = Fr^{-1}\mu(t). \tag{62}$$

The pressure drop $\Delta P_2(t)$ across the two-phase region can be obtained by integrating Eq. (56) from $z = \mu(t)$ to $z = \eta(t)$ as

$$\Delta P_2(t) = \Delta P_{\mathrm{acc1},2}(t) + \Delta P_{\mathrm{acc2},2}(t) + \Delta P_{\mathrm{fric},2} + \Delta P_{\mathrm{grav},2}(t), \tag{63}$$

where

$$\Delta P_{\mathrm{acc1},2} = \int_{\mu(t)}^{\eta(t)} \rho_{\mathrm{m}}(z,t)\frac{\partial v_{\mathrm{m}}(z,t)}{\partial t}\,\mathrm{d}z = \left[\frac{\mathrm{d}v_{\mathrm{inlet}}(t)}{\mathrm{d}t} - N_{\mathrm{pch2}}\frac{\mathrm{d}\mu(t)}{\mathrm{d}t}\right]M_1(t), \tag{64}$$

$$\Delta P_{\mathrm{acc2},2} = \int_{\mu(t)}^{\eta(t)} \rho_{\mathrm{m}}(z,t)v_{\mathrm{m}}(z,t)\frac{\partial v_{\mathrm{m}}(z,t)}{\partial z}\,\mathrm{d}z = v_{\mathrm{inlet}}(t)N_{\mathrm{pch2}}(t)M_1(t) + N_{\mathrm{pch2}}^2(t)M_2(t), \tag{65}$$

$$\Delta P_{\mathrm{fric},2} = \int_{\mu(t)}^{\eta(t)} N_{f2}\rho_{\mathrm{m}}(z,t)v_{\mathrm{m}}^2(z,t)\,\mathrm{d}z = N_{f2}[v_{\mathrm{inlet}}^2(t)M_1(t) + 2v_{\mathrm{inlet}}(t)N_{\mathrm{pch2}}M_2(t) + N_{\mathrm{pch2}}^2M_3(t)], \tag{66}$$

$$\Delta P_{\mathrm{grav},2} = \int_{\mu(t)}^{\eta(t)} Fr^{-1}\rho_{\mathrm{m}}\,\mathrm{d}z = Fr^{-1}M_1(t) \tag{67}$$

and $M_3(t)$ in Eq. (66) is

$$M_3(t) = \int_{\mu(t)}^{\eta(t)} \rho_{\mathrm{m}}(z,t)[z - \mu(t)]^2\,\mathrm{d}z. \tag{68}$$

By substituting Eq. (48) into Eq. (57) and integrating it from $z = \eta(t)$ to $z = 1$, we can obtain the pressure drop $\Delta_1 P(t)$ across the superheated vapor region as

$$\Delta P_1(t) = \Delta P_{\mathrm{acc},1}(t) + \Delta P_{\mathrm{fric},1}(t) + \Delta P_{\mathrm{grav},1}(t), \tag{69}$$

where

$$\Delta P_{\mathrm{acc},1} = N_\rho[1 - \eta(t)]\left\{\frac{\mathrm{d}v_{\mathrm{inlet}}(t)}{\mathrm{d}t} + N_{\mathrm{pch2}}\left[\frac{\mathrm{d}\eta(t)}{\mathrm{d}t} - \frac{\mathrm{d}\mu(t)}{\mathrm{d}t}\right]\right\}, \tag{70}$$

$$\Delta P_{\mathrm{fric},1} = N_\rho N_{f1}\{v_{\mathrm{inlet}}(t) + N_{\mathrm{pch2}}[\eta(t) - \mu(t)]\}^2[1 - \eta(t)], \tag{71}$$

$$\Delta P_{\mathrm{grav},1} = N_\rho Fr^{-1}[1 - \eta(t)]. \tag{72}$$

In addition the inlet and outlet pressure drops for the channel are defined respectively as

$$\Delta P_{\mathrm{inlet}}(t) = k_{\mathrm{inlet}} v_{\mathrm{inlet}}^2(t), \tag{73}$$

$$\Delta P_{\mathrm{exit}}(t) = k_{\mathrm{exit}} N_\rho \{v_{\mathrm{inlet}}(t) + N_{\mathrm{pch2}}[\eta(t) - \mu(t)]\}^2, \tag{74}$$

where k_{inlet} and k_{exit} are respectively the inlet and exit pressure loss coefficients.

Substituting the above pressure drop expressions into the following equation for the total external pressure drop

$$\Delta P_{\mathrm{ext}} = \Delta P_1(t) + \Delta P_2(t) + \Delta P_3(t) + \Delta P_{\mathrm{inlet}}(t) + \Delta P_{\mathrm{exit}}(t), \tag{75}$$

we can obtain the final ODE for $v_{\mathrm{inlet}}(t)$ as

$$\frac{\mathrm{d}v_{\mathrm{inlet}}(t)}{\mathrm{d}t} = \frac{1}{f_7(t)}[f_8(t) + f_9(t)f_1(t) + f_{12}(t)f_{13}(t)], \tag{76}$$

where

$$f_7(t) = M_1(t) + \mu(t) + N_\rho[1 - \eta(t)], \tag{77}$$

$$\begin{aligned} f_8(t) = {} & \Delta P_{\mathrm{ext}} - \Delta P_{\mathrm{inlet}}(t) - \Delta P_{\mathrm{exit}}(t) - \Delta P_{\mathrm{fric},3}(t) \\ & - \Delta P_{\mathrm{grav},3}(t) - \Delta P_{\mathrm{acc2},2}(t) - \Delta P_{\mathrm{fric},2} \\ & - \Delta P_{\mathrm{grav},2}(t) - \Delta P_{\mathrm{fric},1}(t) - \Delta P_{\mathrm{grav},1}, \end{aligned} \tag{78}$$

$$f_9(t) = N_{\mathrm{pch2}}\{M_1(t) + N_\rho[1 - \eta(t)]\}, \tag{79}$$

$$f_{12}(t) = \frac{\mathrm{d}\eta(t)}{\mathrm{d}t}, \tag{80}$$

$$f_{13}(t) = -N_{\mathrm{pch2}} N_\rho[1 - \eta(t)]. \tag{81}$$

Now we have obtained the seven ODEs, i.e., Eqs. (10), (11), (31), (32), (46), (47), (76), which compose the dynamic system describing the unsteady flow in the channel.

2.2. The method of solution for the SB

The dynamic system obtained above can be represented as

$$\dot{\boldsymbol{X}}(t) = \boldsymbol{F}(\boldsymbol{X}, \boldsymbol{\gamma}), \tag{82}$$

where the vector of phase variables $\boldsymbol{X}(t)$ is

$$\boldsymbol{X}(t) = (a_1, a_2, s_1, s_2, b_1, b_2, v_{\mathrm{inlet}})^{\mathrm{T}} \tag{83}$$

and the vector of system operating parameters $\boldsymbol{\gamma}$ is

$$\boldsymbol{\gamma} = (N_{\mathrm{sub}}, N_{\mathrm{pch1}}, N_{\mathrm{pch2}}, N_{\mathrm{pch3}}, \Delta P_{\mathrm{ext}})^{\mathrm{T}}. \tag{84}$$

The other parameters in the dynamic system are taken as design parameters.

The local stability of a stationary point for the dynamic system is determined by the real parts of the seven eigenvalues λ of the Jacobian matrix

$$\boldsymbol{J} = \boldsymbol{F}_{\boldsymbol{X}}(\widetilde{\boldsymbol{X}}, \boldsymbol{\gamma}) \tag{85}$$

which is evaluated at the stationary point. If all the seven eigenvalues have negative real parts, then the stationary point is stable [9].

It is well known that the SB for density wave oscillations are made of Hopf bifurcation points which are characterized by a simple pair of purely imaginary eigenvalues $\pm \mathrm{i}\beta$ of the Jacobian $\boldsymbol{J}$, hence we can simply obtain the SB from the steady-state equations for the dynamic system and the two supplemental equations provided by setting the real and imaginary parts of the determinant of $\boldsymbol{J} - \mathrm{i}\beta\mathbf{I}$ equal to zero respectively. Here β is the initial oscillation frequency, $\mathbf{I}$ is the identity matrix and i is the imaginary unit.

Since the steady-state solutions for the preceding six-phase variables, i.e., Eqs. (12), (13), (34), (35), (49), (50), can be represented by the seventh phase variable v_{inlet}, therefore the steady-state equations are actually reduced to one steady-state equation, Eq. (75), if we do not count in the solutions for the phase change numbers N_{pch1}, N_{pch2} and N_{pch3} which are provided by our previous steady-state analysis. In all, the SB can be determined by solving the three equations, i.e., Eq. (75) and the two supplemental equations. The three unknowns to be solved are β, ΔP_{ext} and v_{inlet}. A Hopf point can be directly obtained when the solution for the three equations is found. All the Hopf points under a certain studied case, such as the effect of the inlet pressure loss coefficients, connected together constitute the SB for the case.

In this paper the 49 partial derivatives in the Jacobian under any steady state are obtained analytically using the symbolic manipulation package "Mathematica", and the three equations are also solved by the same package. In addition, the Hopf points obtained are checked using BIFPACK, which is a program package specifically developed for continuation, bifurcation, and stability analysis [10]. It can trace a series of stationary solutions (such as decreasing ΔP_{ext} gradually), check its stability automatically for each solution, and identify the type of bifurcation point when it is met. The results shown are exactly the same for the two solving methods, and the bifurcation points for the dynamic system in this paper are indeed the Hopf points of the supercritical nature, which are clearly indicated by BIFPACK.

3. Results and discussions

3.1. Input parameters and some preliminary parameter sensitivity analyses

Table 1 presents the dimension of the annular channel of secondary side and the two ducts of primary side. Table 2 shows the steady-state operation inlet parameters designed for the channel at the pressures of 2, 3, 4 MPa. The outlet parameters calculated from our steady-state model can be referred to Ref. [8]. Some input parameters required to do the SB analysis are summarized in Table 3. It can be seen that the three N_{pch}'s under different working pressures vary little with the inlet velocities. In fact, the relative little changes in value for the N_{pch}'s result from the operation requirement that the primary inlet temperatures are changed linearly with the secondary inlet velocities (see Table 2).

The friction factors for the channel vary actually with the flowing mass rate, but here for simplicity, they are taken invariable as that in Karve's analysis. Hence the typical averaged values $N_{f1} = 12$, $N_{f2} = 22.4$ and $N_{f3} = 20.1$ are used in the following analyses. It can be expected that this approximation method (i.e., taking three invariable friction factors) combined with the parabolic characteristic profile of the variation of external pressure drop with the channel inlet velocity will result in some inaccuracies at small inlet velocities, especially for small inlet throttling coefficients. However, reasonable computation results of the SB over the most range of the inlet velocities or at relative large k_{inlet}'s, which correspondence to relative large ΔP_{ext}'s, can still be anticipated.

It is well known that a narrow boiling channel is more liable to experience instabilities when compared with a boiling channel in conventional dimension. This is identified from the large k_{inlet} values (by the way, they are readily achievable in practical applications) obtained in this paper.

We also carried out some preliminary studies of parameter sensitivity to the SB solved. The effect of the little variation of the phase change numbers on SB is examined by using the two different groups of phase change numbers, i.e., N_{pch1}, N_{pch2}, N_{pch3}, are respectively

Table 1
Dimension of the annular channel and the primary ducts

Height of the channels	L	1.3 m
Inner radius of the inner tube	r_{iwi}	2.5×10^{-3} m
Outer radius of the inner tube	r_{iwo}	4.0×10^{-3} m
Inner radius of the outer tube	r_{owi}	5.0×10^{-3} m
Outer radius of the outer tube	r_{owo}	6.5×10^{-3} m
Inner radius of the outer insulated cylinder	r_e	8.1×10^{-3} m

Table 2
Steady-state operation inlet parameters at all pressures

Primary sides		Secondary side	
m_{if} $(= m_{of}) \times 10^2/(\mathrm{kg\,s^{-1}})$	T_{ifi} $(= T_{ofi})/(^\circ\mathrm{C})$	$m_b \times 10^4/(\mathrm{kg\,s^{-1}})$	v_{inlet}
	286.63	6.2406	0.2
	289.77	15.601	0.5
3.617	292.38	23.402	0.75
	295.00	31.203	1.0
	297.09	37.443	1.2

Table 3
Steady-state parameters for SB analyses

	2 MPa			3 MPa			4 MPa		
v_{inlet}	N_{pch1}	N_{pch2}	N_{pch3}	N_{pch1}	N_{pch2}	N_{pch3}	N_{pch1}	N_{pch2}	N_{pch3}
1.0	8.742	468.201	223.255	5.141	226.866	130.02	3.314	118.833	83.549
0.85	7.694	466.821	225.654	4.473	223.905	130.9	2.909	117.664	84.584
0.6	6.206	464.832	229.815	3.276	223.932	134.215	2.33	115.811	86.398
0.5	5.632	464.229	231.566	2.713	221.559	134.695	2.114	115.142	87.171
0.35	5.035	463.407	234.243	1.847	221.017	136.411	1.888	114.153	88.357
N_{pch} used	5	463.4	234	1.4	221	137	2	114	88.4
N_r	1.012			1.0186			1.0258		
N_{sub}	21.603 (at $T_{bi} = 100\,^\circ\mathrm{C}$)			17.599 (at $100\,^\circ\mathrm{C}$)			15.047 (at $100\,^\circ\mathrm{C}$)		
v_0 (m/s)	0.129846			0.134231			0.138174		
Fr	0.00132204			0.00141282			0.00149707		

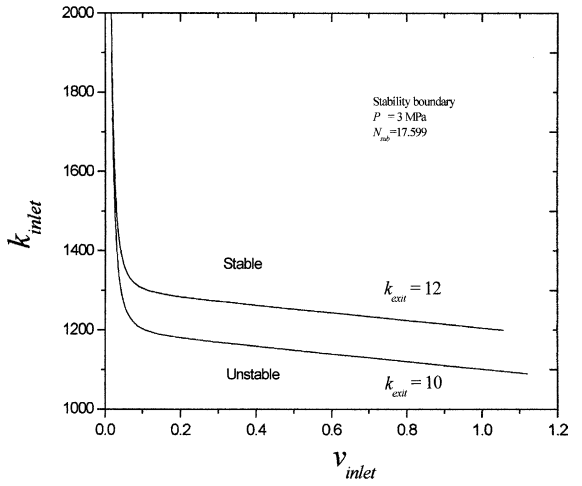

Fig. 2. The effects of k_{inlet} and k_{exit} on SB.

1.4, 221, 137 and 5.141, 226.87, 130.02 at 3 MPa. The comparison of the results shows that the differences between two groups of results are very small and the effect can be neglected. When taking N_{pch1}, N_{pch2}, N_{pch3} respectively as 1.4, 221, 137 and 5, 221, 137 at 3 MPa, the results are totally the same for the two groups of phase change numbers. It indicates that the effect of the variation of N_{pch1} is the least among the three. Therefore N_{pch1}, N_{pch2}, and N_{pch3} can be taken invariable respectively as given in Table 3.

It is found that the most sensitive parameter to SB is N_r, especially when k_{inlet} is small. For example, for the upper curve in Fig. 2 when k_{inlet} is kept at 1200 and N_r taken as 1.0186, the v_{inlet}, on the SB is 1.05539, but if N_r is taken as 1.019 and 1.02 for the same situation, the results of v_{inlet} are respectively changed to 0.784074 and 0.158424. However, when k_{inlet} is kept at 1600 and N_r taken respectively as 1.0186, 1.019 and 1.02, the results obtained are 0.0246629, 0.023898 and 0.0224636. The differences between the three v_{inlet}'s are narrowed. The reason why the significant digits of N_r at a small k_{inlet} have so much influence on the results obtained is that they affect the ΔP_{ext} profile much apparently for a small k_{inlet} while the approximation of invariable friction factors is less accurate. Therefore more significant digits should be kept for N_r for a small k_{inlet} in order to obtain a more exact ΔP_{ext} and reduce the effect of approximation of invariable friction factors.

3.2. Effects of varying the inlet and outlet pressure loss coefficients on the SB

The determination of the appropriate k_{inlet} and the effect of k_{exit} on SB are very important to prevent the density wave instability. It is shown in Fig. 2 that a larger k_{inlet} will ensure a more stable operation state, thus increasing k_{inlet} is stabilizing, while increasing k_{exit} is destabilizing since it reduces the stable region. The little k_{exit} in value can also achievable by reducing outlet throttling as much as possible. Although the results generally are in agreement with experimental and analytical findings of earlier investigators, there are still some points needed to be stated. One is that the unstable region still exists for a smaller inlet velocity however large the k_{inlet} is. This reveals that for the range of parameters studied in this paper, the dynamic system model developed at the present work manifests mathematically well the characteristic of the unstable flow boiling. Another point is the shapes of the two SB's in the figure are relatively flat, which means increasing k_{inlet} beyond a certain level (at what value of the level is the most important concern for a practical application) will ensure most of the working range in stable region. Besides, the sensitivity of the SB to k_{exit} is also strong especially for a small k_{inlet}, which can also be explained from the relative large extent of the effect of k_{exit} on ΔP_{ext} when the k_{inlet} is small.

3.3. Effects of varying the inlet subcooling number on the SB

The variations of three stability boundaries, respectively for three values of k_{inlet} with inlet subcooling number are shown in Fig. 3. It indicates that if the inlet throttling coefficient is large enough, then the variation of the inlet subcooling number does not have much influence on the SB; but with the reduction of the inlet throttling coefficient the SB will gradually change its shape into a parabolic curve, which means for a certain inlet velocity the flow will only be stable under a small N_{sub} or over a large N_{sub} but between them the flow will be unstable.

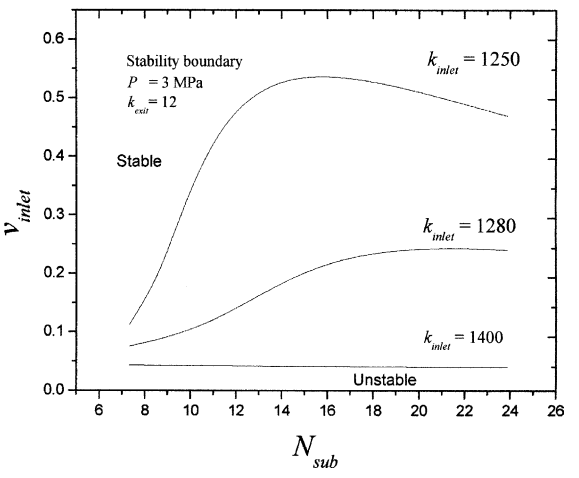

Fig. 3. The effects of N_{sub} on SB.

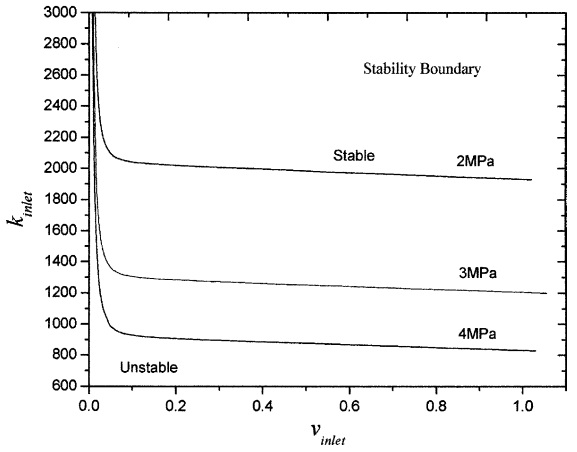

Fig. 4. The effects of system pressure on SB.

The N_{sub} range studied in the figure is from 7.32 to 23.88, which correspondes to the range of inlet temperature from 180 to 50 °C.

3.4. Effect of system pressure on the SB

As shown in Fig. 4, increasing the system pressure will enlarge the stable region, thus is stabilizing. The effect is similar to decreasing the outlet throttling coefficient. Although the reference velocities for the three system pressures are a little different (see Table 3) in Fig. 4, the comparison is still meaningful. The result of the effect of system pressure is also in agreement with previous findings of other researchers.

4. Conclusions

The model developed in this paper describing the forced-flow water boiling in a concentric circular-tube narrow annulus heated by primary countercurrent water from the inner surface and the outer surface simultaneously can manifest well the unstable flow boiling characteristic of density wave type. For the cases studied in present work the phase change numbers for the three regions of the channel can be taken as piecewise constants under different system pressures respectively. Under the approximation of invariable friction coefficients, the more significant digits should be kept for parameter N_r to do the SB analysis, especially when the inlet throttling coefficient is small.

The large k_{inlet} in value obtained in this paper indicates the boiling flow instabilities in a narrow annular channel are indeed more liable to occur compared with a channel in conventional dimension. Increasing inlet throttling coefficient or increasing system pressure is stabilizing while increasing outlet throttling coefficient is destabilizing. The sensitivity of the SB to outlet throttling coefficient is also strong when inlet throttling coefficient is relatively small. Changing inlet subcooling temperature does not have much influence on the SB if the density wave instability is depressed by a large inlet throttling coefficient, yet for a small inlet throttling coefficient the shape of the unstable region will become parabolic.

Acknowledgements

The project was financially supported by the National Natural Science Foundation of China with Grant number 50376032. The author (Hu Yaojiang) is also grateful for the encouragement and a great help from Prof. Huang Suyi at Huazhong University of Science and Technology, and for the partial support related to this work from Research Institute of Nuclear Power Operation, Wuhan, PR China.

References

[1] J.A. Boure, A.E. Bergles, L.S. Tong, Review of two-phase flow instability, Nucl. Eng. Des. 25 (1973) 165–192.
[2] R.T. Lahey, Advances in the analytical modeling of linear and nonlinear density-wave instability modes, Nucl. Eng. Des. 95 (1986) 5–34.
[3] J.L. Achard, D.A. Drew, R.T. Lahey, The analysis of nonlinear density-wave oscillations in boiling channels, J. Fluid Mech. 155 (1985) 213–232.
[4] Rizwan-Uddin, Effects of double-humped axial heat flux variation on the stability of two-phase flow in heated channels, Int. J. Multiphase Flow 20 (1994) 1129–1142.
[5] Rizwan-Uddin, On density-wave oscillations in two-phase flows, Int. J. Multiphase Flow 20 (1994) 721–731.
[6] W. Ambrosini, P. Di Marco, J.C. Ferreri, Linear and nonlinear analysis of density wave instability phenomena, Heat Technol. 18 (2000) 751–760.
[7] A.A. Karve, Nuclear-coupled thermal-hydraulic stability analysis of boiling water reactors. Ph.D. Thesis, 1998, University of Virginia.
[8] Y. Hu, H. Cheng, The steady-state boiling flow in a narrow vertical annulus heated by counterflow fluids from inner and outer surfaces, Int. Commun. Heat Mass Transfer, submitted.
[9] R. Seydel, Practical bifurcation and stability analysis, second ed., Springer-Verlag, New York, 1994.
[10] R. Seydel, A Program Package for Continuation, Bifurcation, and Stability Analysis, Version 3.3, February 1999.